Journal of Advanced Research 24 (2020) 363–370

Contents lists available at ScienceDirect

Journal of Advanced Research

journal homepage: www.elsevier.com/locate/jare

A novel tetrapeptide fluorescence sensor for early diagnosis of prostate cancer based on imaging Zn^{2+} in healthy versus cancerous cells

Yong An [a], Wei Chang [a], Wei Wang [a], Hao Wu [a], Ke Pu [c], Anhu Wu [a], Ze Qin [a], Yan Tao [a], Zhongjin Yue [a,*], Peng Wang [b,*], Zhiping Wang [a,*]

[a] Department of Urology, Institute of Urology, Gansu Nephro-Urological Clinical Center, Key Laboratory of Urological Diseases in Gansu Province, The Second Hospital of Lanzhou University, Lanzhou, Gansu 730030, China
[b] Chemical Synthesis and Pollution Control Key Laboratory of Sichuan Province, College of Chemistry and Chemical Engineering, China West Normal University, Shida Road 1#, Nanchong 637002, China
[c] Department of Gastroenterology, The First Hospital of Lanzhou University, Lanzhou, China

GRAPHICAL ABSTRACT

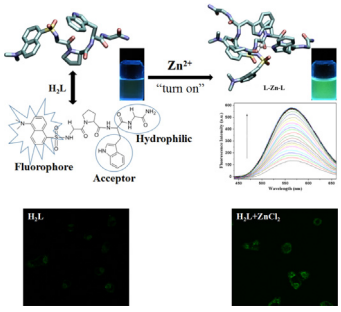

ARTICLE INFO

Article history:
Received 24 January 2020
Revised 23 March 2020
Accepted 15 April 2020
Available online 28 April 2020

Keywords:
Peptide
Fluorescent sensor
Zn^{2+} ions
Prostate cancer cells
Imaging diagnosis

ABSTRACT

Zinc as a biomarker can be used to diagnose the early stage prostate cancer, while ZIP1 protein, a zinc transporter is significantly down-regulated in prostate cancer cells. This behavior leads to the apparent alteration of the enrichment ability for zinc between early prostate cancer tissues and healthy tissues. This difference inspires us to develop a novel Zn^{2+} sensor that applies to the clinic diagnosis of early prostate cancer. We designed a tetrapeptide sensor **H_2L** (Dansyl-Gly-Pro-Trp-Gly-NH_2) according to the photo-induced electron transfer principle (PET), and it performed adequately in Zn^{2+} imaging of prostate cell lines. Based on the assessment of Zn^{2+} enrichment ability, there was distinctly lower Zn^{2+} concentrate in prostate cancer cell lines than healthy prostate epithelial cells. Furthermore, **H_2L** displayed high sensitivity with a detection limit as low as 49.5 nM, and high specificity for Zn^{2+} detection. Also the low toxicity and the superior cell permeability of **H_2L** made the imaging of Zn^{2+} ions detection safe and rapid. We expect that **H_2L** to be a powerful tool for early diagnosis of prostate cancer and a good indicator for the precise resection of cancer tissue during surgery.
© 2020 Production and hosting by Elsevier B.V. on behalf of Cairo University. This is an open access article under the CC BY-NC-ND license (http://creativecommons.org/licenses/by-nc-nd/4.0/).

Introduction

Prostate cancer is the second most common tumor in the elderly [1]. Early intervention using radical prostatectomy can significantly increase the cure rate [2]. Therefore, methods that

Peer review under responsibility of Cairo University.
* Corresponding authors.
E-mail addresses: yuezhongjin@sina.cn (Z. Yue), wangpchem17@163.com (P. Wang), wangzplzu@163.com (Z. Wang).

https://doi.org/10.1016/j.jare.2020.04.008
2090-1232/© 2020 Production and hosting by Elsevier B.V. on behalf of Cairo University.
This is an open access article under the CC BY-NC-ND license (http://creativecommons.org/licenses/by-nc-nd/4.0/).

reliably diagnose early prostate cancer and improve the cure rate of advanced prostate cancer remained critical hotspots. At present, common practiced screening methods for early prostate cancer are serum prostate-specific antigen (PSA) blood test and digital rectal palpation [3–5]. In case of an elevated value of PSA, diagnostic imaging examinations (CT or MRI) are needed [5]. Nevertheless, the aforementioned screening methods lack adequate sensitivity for the early prostate cancer diagnosis [6]. Tissue biopsy, as a standard reference, is regarded as the only method for cancer diagnosis [5]. At the moment, the false-positive of PSA reaches 75%. This high rate of error leads to unnecessary biopsy and excessive therapy [7,8]. Therefore, the development of new diagnostic biomarkers for prostate cancer is much needed.

Zinc is involved in many critical physiological pathways in the human body [9,10]. According to the study of Franz and his colleagues, there was about 2–4 g of zinc in the human body, which distributed mainly from the organs such as prostate, eyes, brain, semen, bones, muscles, kidneys and liver. In particular, the prostate tissue has the highest zinc content approximated to 3–10 fold than other tissues [11]. Zn^{2+} ions are closely associated with the carcinogenesis of prostate cancer. Many studies had reported that the zinc concentration of prostate periphery, a cancerous region, reduced six-fold in prostate cancers compared with normal prostate periphery during the process of prostate cancer development [7,12,13]. Of note, this differential alteration of zinc content started from the early stages of prostate cancer due to the abnormal expression of hZIP1, which is a specific zinc transporter [2,14,15]. As there is no similar trend observed in the prostatitis and benign prostatic hyperplasia [16]. Prostate cancer is the only prostate diseases to lose the ability of the Zn^{2+} accumulation. Therefore Zn^{2+} can be used as a specific biomarker for the early diagnosis of prostate cancer.

Traditional methods for Zn^{2+} detection have many disadvantages in the ability of diagnostic accuracy, diagnostic speed and location imaging. With the burgeoning development of new fluorescent chromophore labelling techniques, various types of fluorescent sensors have been developed [17–24]. Among them, peptide sensors have many advantages including high sensitivity, easy detection, low biological toxicity and convenient synthesis. They also have better attractive feature compared with other kinds of fluorescence sensors [24–26]. Currently, several peptide-based fluorescent sensors for Zn^{2+} detection had been developed [26–29], based on the specific Zn^{2+}-binding domains in the amino acid side chains of aspartic acid, glutamic acid, cysteine and histidine [26]. However, these reported articles mainly focused on the cell imaging of the sensor rather than a clinical application for diseases diagnosis. Moreover, at present, few articles explore the clinical application of Zn^{2+} sensor for prostate malignancy [2,15,30].

In this paper, we designed and synthesized a novel fluorescent sensor **H_2L** (Dansyl-Gly-Pro-Trp-Gly-NH_2) with tryptophan and dansyl fluorophore group. In this sensor **H_2L**, the fluorophore (electron acceptor) is provided by the dansyl group, the Pro-Gly structure is the linker, and tryptophan (Try) is the binding group, the peptide-based chemosensors contain a β-turn (Pro-Gly) motif instead of a loop domain in metal ion binding protein and special amino acids in the binding site. **H_2L** displayed a fast fluorescence "turn-on" response toward Zn^{2+} selectively. The fluorescence of **H_2L** held in quenched status due to the inhibition of photo-induced electron transfer principle (PET) between tryptophan and dansyl chloride group. As shown in Scheme 1, when the receptor region of **H_2L** combines with Zn^{2+} ions, the electron transfer process is interrupted, resulting in fluorescence recovery. The Job's plot and fluorescence titration methods were used to determine the binding mode of **H_2L** to Zn^{2+} as 2:1. The detection limit for Zn^{2+} of the proposed assay is 49.7 nM. Furthermore, **H_2L** has advantages of low toxicity for cells, high sensitivity and specificity for the detection of Zn^{2+}. In the assessment of potential bio-imaging assays, the results identified that not only **H_2L** could visualize intracellular Zn^{2+} successfully, it also reflects the differential concentration of Zn^{2+} in prostate cancer cells and prostate healthy epithelial cells.

Materials and methods

Materials and instruments

Reagents used for synthesis were purchased from the corresponding reagent companies and used without further purification. Antibody used for Western blotting experiments were supplied by Abcam (U.K.), Cell Counting Kit-8 for cytotoxicity test (Dojindo, Japan). Cells were obtained from the Chinese Academy of Sciences (CAS), culture medium and serum (Thermo Fisher Scientific, USA). Mass spectra (MS) were measured on a Bruker Daltonics Esquire 6000 spectrometer. Recording all pH buffers by using a pHS-3E digital pH meter. UV–vis absorption spectra were measured by an AVARIAN UV-Cary100 spectrophotometer. Fluorescence emission spectra were measured using a Cary Eclipse fluorescence spectrophotometer. LSM 710 inverted fluorescence microscope (Carl Zeiss, Germany) was used for cell imaging. Fluorescent photographs of the samples were taken under a UV lamp at 365 nm. ImageJ software (USA) was used for cell fluorescence quantification and analysis of protein immunoblot results.

*Synthesis of **H_2L***

The probe **H_2L** was synthesized using the solid phase peptide synthesis (SPPS) technology. We detailed the specific synthesis steps in Supporting Information.

General fluorescence measurements

Due to the outstanding water solubility of **H_2L**, **H_2L** was prepared to a concentration of 10^{-3}mM using distilled water. Metal salts (Ag^{+}, Al^{3+}, Ca^{2+}, Cd^{2+}, Co^{2+}, Cr^{3+}, Cu^{2+}, Fe^{2+}, Fe^{3+}, Hg^{2+}, K^{+}, Mg^{2+}, Mn^{2+}, Na^{+}, Ni^{2+}, Pb^{2+}, Zn^{2+}) were prepared as stock solutions at a concentration of 10^{-3}mM also using distilled water. Fluorescence experiments were performed in HEPES buffer solutions (10 mM, pH = 7.4). The excitation and emission slit widths were 10.0 nm. For the dansyl group, the concentration of **H_2L** was confirmed by UV absorbance at 330 nm.

Cell culture

The early stage of prostate cancer cell model (LNCaP) and bladder cancer cell (T24) were cultured in RMPI-1640 medium. The castration-resistant prostate cancer cell model (PC-3) was cultured in F12K medium. The prostate healthy epithelial cell (RWPE-1) and bladder healthy epithelial cell (SV-HUC-1) were cultured in DMEM (37 °C, 5% CO_2). All culture medium contained 10% fetal bovine serum.

Cytotoxicity test

Cells were seeded at a density of 1×10^4 cells/ml per well in 96-well plates and incubated at 37C in a 5% CO_2 incubator for 72 h. At 24 h, cells were co-cultured with **H_2L** at concentrations from 0 to 160 μM for 48 h, respectively. The viability of the cells was measured with a cell counting Kit-8 after 72 h.

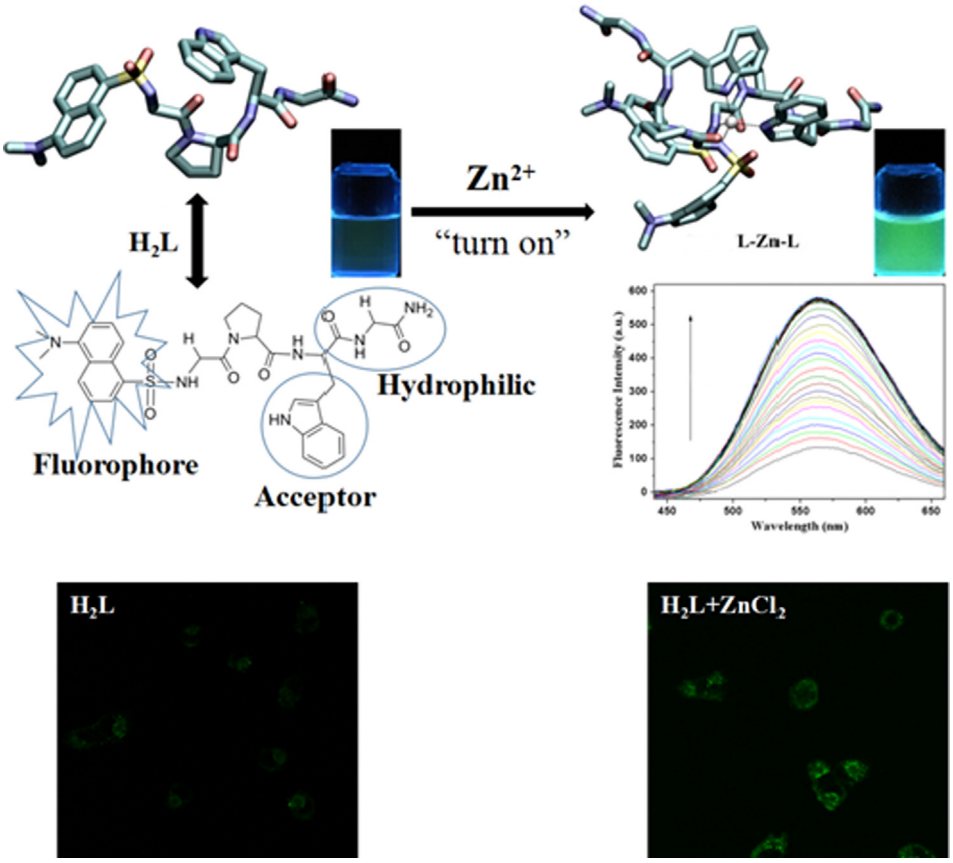

Scheme 1. Schematic diagram of sensor **H_2L** for Zn^{2+} detection.

Real-time PCR

Total intracellular RNA was extracted using Trzol and reverse-transcribed into cDNA, and primer sequences for target genes were designed by Oligo7 software (Table S2). The prepared cDNA was subjected to PCR amplification with a program consisting of 40 cycles of 95 °C for 30 s, followed by 95 °C for 5 s, 60 °C for 30 s. β-actin was used as an internal reference. Relative levels of mRNA transcription were calculated using the $2^{-\Delta\Delta CT}$ method.

Western blot

Cells were added with the lysis solution RIPA (containing 1% PMSF) and left to lyse on ice for half an hour, and then the EP tubes were placed into a 4 °C icebox for sonication for 2 min, followed by centrifugation at 12,000 r/min for 20 min. The supernatant was taken and moved to a new EP tube, and the protein concentration was measured using a BCA kit. And then 5-fold loading buffer was added, and the solution was kept in a boiling water bath for 10 min and stored at −20 °C after aliquoting for future use. Proteins were separated by using SDS-PAGE, and then were transferred to PVDF membranes, 5% non-fat milk was added into the PVDF membranes to block non-specified proteins for one hour before hZIP1 (SLC39A1) antibody and β-actin antibody with a concentration of 1:1000 were incubated with PVDF membranes for overnight at 4 °C. The secondary antibodies of goat anti-mouse and goat anti-rabbit were used to the twice incubation with 1:10,000 for 40 min at room temperature. Finally the bands were exposed by using the Odessey detection system. β-actin was the internal reference protein. The grey values of the bands were measured by using ImageJ software, and the results of hZIP1 protein expression were expressed as the ratio of the grey values of both hZIP1 and β-actin protein bands.

Procedures for intracellular Zn^{2+} imaging

Cells were seeded at a density of 1×10^4 in 20-mm-diameter dishes, and the next day the medium was removed and co-cultured for 24 h with serum-free medium containing $ZnCl_2$ (50 μM) or no $ZnCl_2$. After 24 h, **H_2L** (10 μM) was added after three washes with PBS and incubated for 30 min, followed by the addition of TPEN (100 μM) for a further one hour in some dishes after 30 min. These cells had been washed and replaced with a fresh medium before imaging. Quantitative fluorescence analysis of the cells was performed using ImageJ software.

Results and discussion

*The fluorescence emission spectroscopy of **H_2L** to Zn^{2+}*

The prominent water solubility of the peptide sensor **H_2L**, was the foundation for the experiments of HEPES buffer solutions (pH = 7.4, 10 mM). The fluorescence spectra of **H_2L** combined with various metal ions (Ag^+, Al^{3+}, Ca^{2+}, Cd^{2+}, Co^{2+}, Cr^{3+}, Cu^{2+}, Fe^{2+}, Fe^{3+}, Hg^{2+}, K^+, Mg^{2+}, Mn^{2+}, Na^+, Ni^{2+}, Pb^{2+}, Zn^{2+}) were investigated and analyzed individually. Notably, **H_2L** showed specific selectivity for Zn^{2+} ions, as the other metal ions did not provide a similar outcome (Figs. 1A and S6). **H_2L** emitted the weak fluorescence inhibited by PET from tryptophan to dansyl group. When 1.0 equivalents of various metal ions were added separately to the **H_2L** solutions, the fluorescence of **H_2L** was significantly enhanced about five times when Zn^{2+} ions rather than other metal ions were

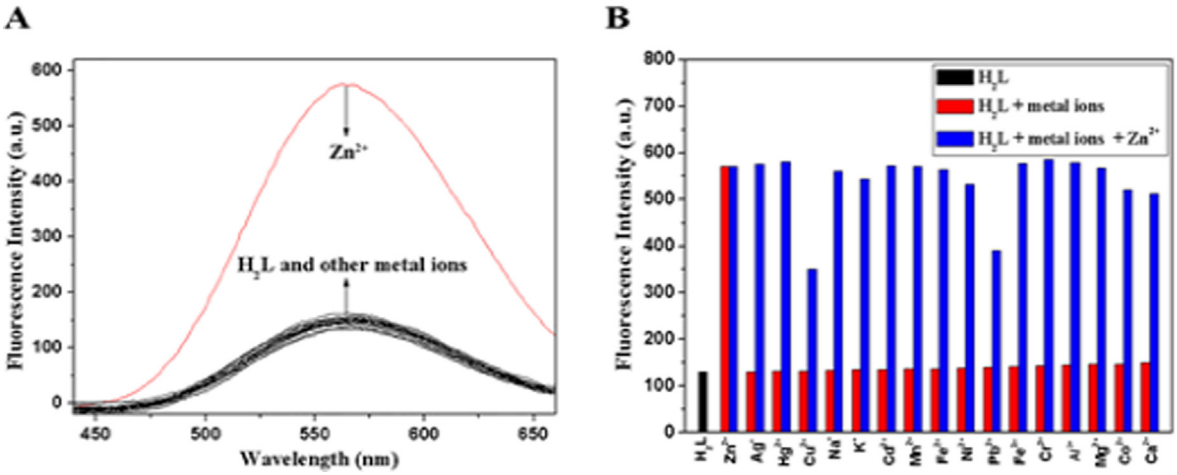

Fig. 1. (A) Fluorescence spectrum changes of **H_2L** (10.0 uM) after adding 1.0 equivalent of various metal ions (Ag^+, Al^{3+}, Ca^{2+}, Cd^{2+}, Co^{2+}, Cr^{3+}, Cu^{2+}, Fe^{2+}, Fe^{3+}, Hg^{2+}, K^+, Mg^{2+}, Mn^{2+}, Na^+, Ni^{2+}, Pb^{2+}, Zn^{2+}). (B) Fluorescence intensity detection of **H_2L** (10 uM) and its complexation with Zn^{2+} ions (1.0 equiv.) in the presence of other metal ions (5.0 equiv.).

added into this solution, which was due to the combination of Zn^{2+} ions with **H_2L** resulting in the interruption of PET.

It was inevitable that the anti-interference ability of sensors was assessed in biological detection. The anti-interference ability of **H_2L** for Zn^{2+} ions detection were evaluated in the presence of other metal ions. The results showed that other metal ions except for copper ions did not interfere with the **H_2L** detection for Zn^{2+} ions. As the paramagnetic effect of Cu^{2+}, the fluorescence of **H_2L** was quenched mildly. However, this interference was limited and did not affect the detection of **H_2L** for Zn^{2+} ions (Figs. 1B and S6). In conclusion, sensor **H_2L** has good anti-interference ability and could apply for the detection of Zn^{2+} ions in complex organisms.

Binding mode of H_2L with Zn^{2+}

The binding ratio of sensor **H_2L** to Zn^{2+} ions was investigated by using fluorescence titration experiments. We recorded the results of the fluorescence response of **H_2L** with different concentrations of Zn^{2+} in HEPES buffer solutions (10.0 mM, pH = 7.4) at an excitation wavelength of 330 nm. We can observe that the fluorescence intensity of **H_2L** reached the highest peak at 560 nm (Fig. 2A), when the amount of Zn^{2+} was adjusted to 0.5 equiv. the **H_2L** solution changed from colourless to green in the fluorescence cuvette under a 365 nm UV lamp (Fig. 2B inset). With a burgeoning amount of Zn^{2+} ions, the titration curve arrived at a stable plateau (Fig. 2B), which implied that the ratio of **H_2L** and Zn^{2+} ions was 2:1.

To further investigate binding stoichiometry, Job's plot analysis was performed. The concentration of **H_2L** and Zn^{2+} ions were appropriately adjusted to keep the total concentration of a solution as constant. When the fluorescence intensity reached to the maximum value, the mole fraction of Zn^{2+} was 0.33 (Fig. 2C). The results further indicated that the binding ratio of **H_2L** to zinc was 2:1. Additionally we calculated the binding constant of **H_2L** to Zn^{2+} was 8.18×10^8 M^{-2} based on the stoichiometry results (Fig. S3). The detection limit of **H_2L** for Zn^{2+} was calculated to be 49.7 nM according to the specific formula (Fig. S4). This result suggested that **H_2L** had the potential to detect low levels of Zn^{2+} ions in organisms.

Theoretical calculations were essential for the study of the structure of **H_2L** and **L-Zn-L** complexes, and understood the specific recognition of **H_2L** for Zn^{2+} ions. We performed a density functional theory (DFT) calculations on **H_2L** and **L-Zn-L** complexes systems using the Gaussian 09 software [31]. At the B3LYP/6-31G (d) level [31,32], the geometry and energy minimum optimization of **L-Zn-L** complexes structure were carried out, and We obtained the optimized configuration of **H_2L** and **L-Zn-L** complexes systems [33,34] (Fig. 2D). As shown as in Fig. 2D, zinc ions could coordinate with the four nitrogen atom groups of two **H_2L** to form **L-Zn-L** complexes. The lowest energy and the stable structure were reached by combining with the coordination ratio (**H_2L** = 41.111 k cal/mol, **L-Zn-L** = 105.104 kcal/mol).

Interference of pH and amino acids

The pH value of the organism was waving from 7.0 to 7.4, the sensor detected Zn^{2+} ions in vivo depended on whether this range of pH value could influence the sensor detection for Zn^{2+}. Interference of pH test was conducted in the aqueous solutions with different pH value (2.0–12.0). The results illustrated that the fluorescence intensity of **H_2L** showed weak enhancement from pH 5.0 to 12.0 in the solutions without Zn^{2+}, but **H_2L** reflected the highly efficient fluorescence response to Zn^{2+} solutions from pH 6.0 to 10.0 (Fig. 3A). Therefore, **H_2L** could endure the environment in the human body and perform as intended.

The interference studies of **H_2L** with amino acids (His, Cys, Trp, Gly, Ala, Val, Leu, Ile, Pro, Phe, Tyr, Ser, Thr, Met, Asn, Gln, Asp, Glu, Lys and Arg) were performed in HEPES buffer solutions (10.0 mM, pH = 7.4). As shown in the Fig. 3B, there was no obvious changes of fluorescence intensity could be observed when 5.0 equiv. other amino acids were added into the relevant solutions except for histidine, cysteine and tryptophan. We speculated that the combination of these three amino acids and Zn^{2+} ions leads to a decrease in fluorescence. The results indicated that the fluorescent probe **H_2L** could be applied to selectively recognize Zn^{2+} ions in complex environment.

Reaction time, reversibility and biological toxicity test

To rapid detection was an essential condition for sensors as clinical diagnostic tools. Reaction time test showed the fluorescence intensive of **H_2L** significantly heightened within 20 s and reached to a plateau from 20 s to 300 s after Zn^{2+} interference (Fig. 3C). The experimental result exhibited **H_2L** could provide rapid response to Zn^{2+}. Furthermore, the results of fluorescence stability test showed the fluorescence intensity of the complex could maintain 6 h (Fig. S5). Accordingly, it was a promising

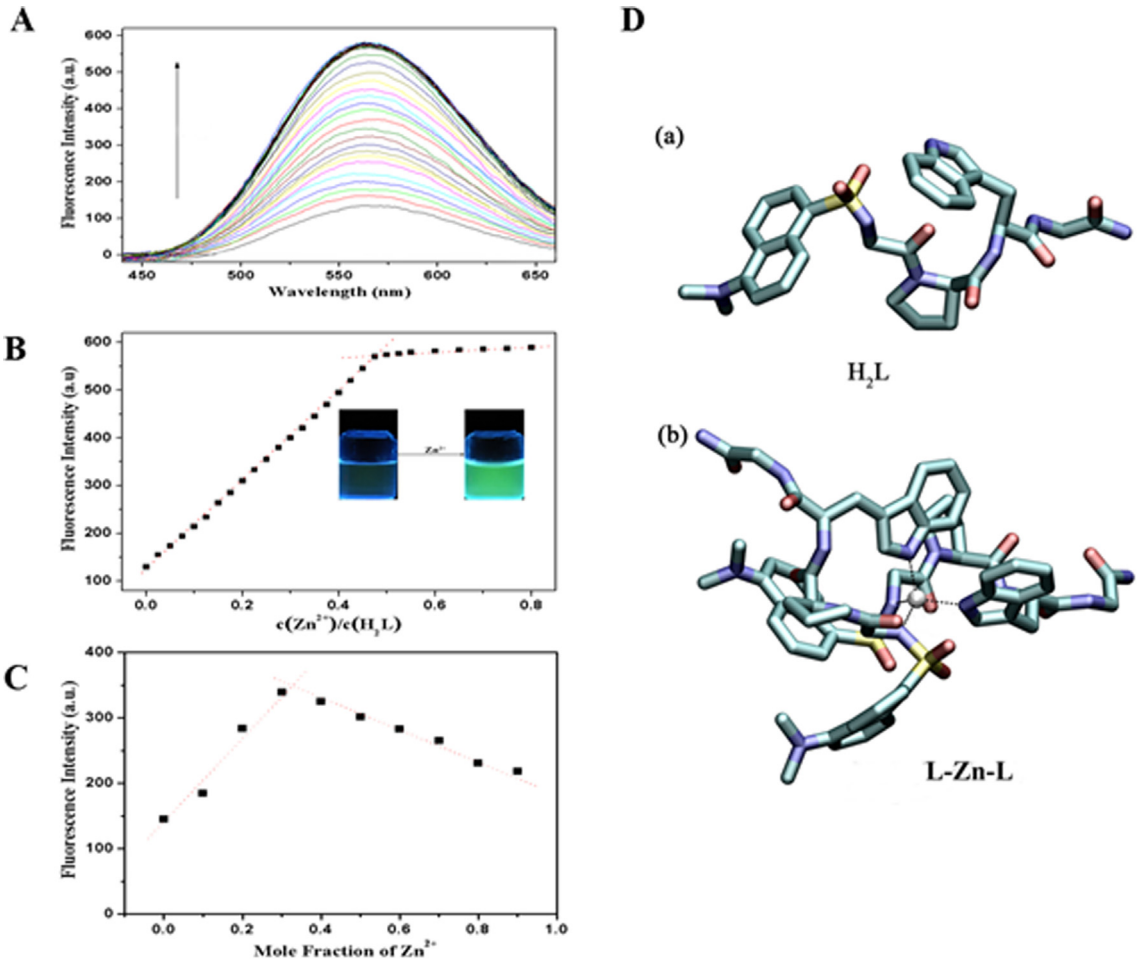

Fig. 2. (A) Fluorescence emission spectra of **H_2L** (10.0 μM) with various amounts of Zn^{2+} (0–0.80 equiv.). (B) Fluorescence intensity changes of **H_2L** (10.0 μM) with various amounts of Zn^{2+}. The inset is: **H_2L** aqueous solution changes from colorless to green (UV lamp, 365 nm) after addition of 0.5 equiv of Zn^{2+} ions. (C) Job's plot to determine the stoichiometry of **H_2L** versus Zn^{2+} ions (λex = 330 nm). The total [**H_2L**] + [Zn^{2+}] = 10.0 μM. (D) Calculated energy-minimized optimized structures for the **H_2L** (a) and **L-Zn-L** complex (b).

indicator to accomplish the rapid diagnosis for tumor screening and precise resection.

The reversibility of **H_2L** (5.0 μM) was performed by adding Zn^{2+} ions (10.0 μM) and EDTA (10.0 μM) in HEPES buffer solutions (10.0 mM, pH = 7.4). As shown in Fig. 3D, H2L exhibited a good fluorescence intensity response toward Zn^{2+} ions and EDTA at least ten cycles with small switchable changes when added Zn^{2+} ions and EDTA alternately. The experimental results indicated that **H_2L** could perform as a reversible fluorescence probe for detecting Zn^{2+}.

According to the above research, the sensing mechanism of **H_2L** toward Zn^{2+} ions was discussed. The fluorescence emission of free **H_2L** was nearly quenched and it was due to the photo induced electron transfer (PET) phenomenon from the lone pair electrons (N atoms) of Trp to the dansyl emitter that was caused. Because the pKa values of Trp residues, the negative charge of side groups of Trp residues must increase with increasing pH, which might enhance the photo induced electron transfer between imidazole groups (Trp) and dansyl groups. Nevertheless, when Zn^{2+} were combined with **H_2L**, two N atoms of the a Trp groups participated in the coordination with Zn^{2+} and formed a 2:1 complex, and the fluorescence of **H_2L** was recovered based on the disappearance of PET mechanism (Scheme S2). Considering the interactions between the peptide and Zn^{2+} also enhanced, resulting in the fluorescence increase of the peptide sensor in the presence of Zn^{2+} in this condition.

The cell cytotoxicity assay was used to evaluate the safety of **H_2L**, LNcaP and PC-3 cells were incubated with **H_2L** (0, 20, 40, 80, 160 μM) at 37° C for 48 h, cells viability was tested using a CCK-8 kit. As shown in Fig. 3E, cells viability had no significant alteration when compared with the control group in different concentrations. This result demonstrated that **H_2L** has low toxicity and can be considered safe for biological imaging.

Real-time PCR and Western blot analysis

The disability of Zn^{2+} enrichment mainly attributed to the down-regulated hZIP1 (SLC39A1) gene in prostate cancer, which plays a crucial role in transporting zinc into the cell [11]. To further explore the correlation between the hZIP1 and Zn^{2+}, we analyzed the mRNA and protein levels of hZIP1 in different cell lines.

The PCR results indicated that the mRNA level of hZIP1 in RWPE-1, healthy prostate cells, was significantly higher than the prostate cancer cells (LNCaP and PC-3) ($P < 0.05$). Similarly, as a control group, bladder healthy epithelial cells SV-HUC-1 also had higher hZIP1 mRNA expression than bladder cancer cells T24 (Fig. 4A) ($P < 0.05$). Western blotting showed hZIP1 protein level of RWPE-1 was elevated obviously compared with LNCaP and PC-3 cells ($P < 0.05$), and the hZIP1 protein expression of SV-HUC-1 was also significantly higher than T24 ($P < 0.05$) (Fig. 4B).

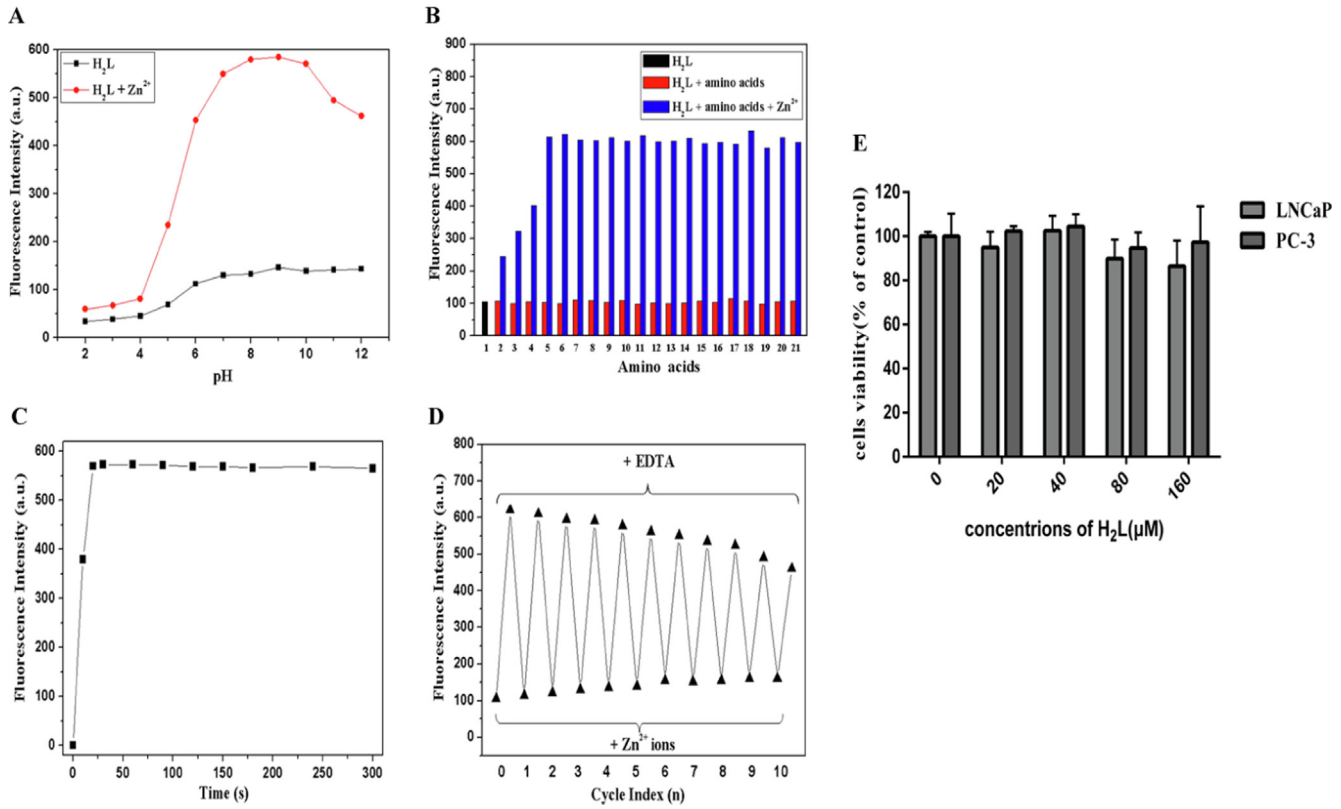

Fig. 3. (A) Effect of different pH value on the fluorescence intensity of **H_2L** (10.0 μM) and **H_2L +** Zn^{2+} (10.0 μM); (B) Fluorescence intensities of **H_2L** (10.0 μM) and its complexation with Zn^{2+} (5.0 μM) in the presence of various amino acids (25.0 μM) in HEPES buffer solutions (10.0 mM, pH = 7.4). (1: L, 2–21: His, Cys, Trp, Gly, Ala, Val, Leu, Ile, Pro, Phe, Tyr, Ser, Thr, Met, Asn, Gln, Asp, Glu, Lys and Arg); (C) Reaction-time profile of **H_2L** (10.0 μM) with Zn^{2+} (10.0 μM); (D) The reversibility experiment of **H_2L** towards Zn^{2+} by adding EDTA in HEPES buffer solutions (10.0 mM, pH 7.4). λex = 330 nm, slit widths: 10 nm/10 nm; (E) Cytotoxicity results of **H_2L** (0–160 μM).

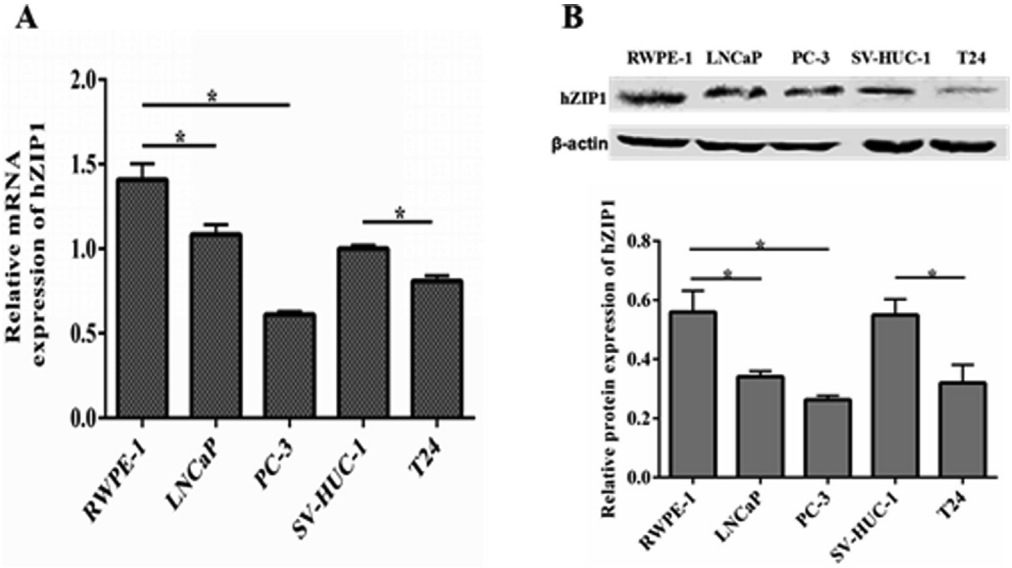

Fig. 4. (A) Real time-PCR results of hZIP1 mRNA expression (B) Western blot for hZIP1 expression, internal control protein was β-actin. * $p < 0.05$, RWPE-I compared with LNCaP and PC-3, and SV-HUC-1 compared with T24.

Therefore, the down-regulated hZIP1 gene might contribute to the diminished ability of prostate and bladder cancer cell lines to enrich Zn^{2+}. Furthermore, our study also demonstrated that hZIP1 might act as a tumor suppressor gene in prostate and bladder cell lines.

Intracellular Zn^{2+} imaging for the diagnosis of prostate cancer

In order to explore the ability of Zn^{2+} enrichment in the cancer cell lines and healthy cells, Zn^{2+} sensing imaging was carried out in cell lines using **H_2L**. Cells were firstly cultured in medium with

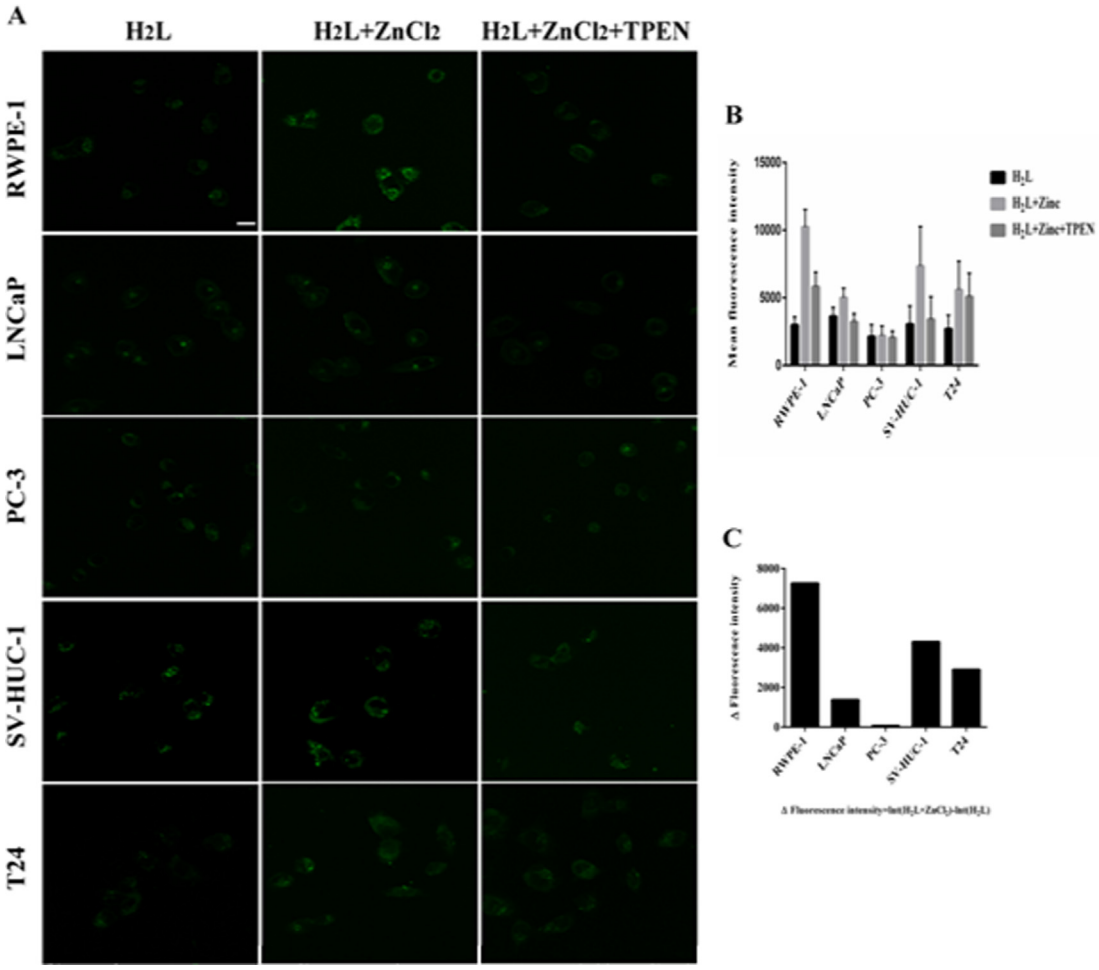

Fig. 5. (A) Fluorescence confocal microscopy of five cell lines. From left to right, respectively, cells were incubated for 30 min with **H_2L** (10 μM); preconditioned with $ZnCl_2$ (50 μM, 24 h) and incubated for 30 min with **H_2L** (10 μM); preconditioned with $ZnCl_2$ (50 μM, 24 h) and incubated for 30 min with **H_2L** (10 μM), followed by incubation for 30 min with the zinc chelator TPEN (100 μM). Scale bar = 20 μm. (B) Cell quantitative fluorescence results. (C) The difference in fluorescence intensity between the **H_2L** + **$ZnCl_2$** group and the **H_2L** group for each cell, represents the ability of different cells to accumulate Zn^{2+}. **Δ Fluorescence intensity = Int (**H_2L** + **$ZnCl_2$**)-Int (**H_2L**).

$ZnCl_2$ (50 μM) or no $ZnCl_2$ for 24 h, and then co-incubated with **H_2L** for 30 min before the confocal fluorescence microscopy test. Imaging results showed that the fluorescence intensity of the prostate healthy cell RWPE-1 was stronger than prostate cancer cells LNCaP and PC-3 in groups treated with Zn^{2+}. In the control group, we observed similar results that the fluorescence intensity of the healthy bladder epithelial cell SV-HUC-1 was stronger than the bladder cancer cell T24 in groups treated with Zn^{2+}. Although there was a lower concentration of Zn^{2+} in tumor cells when compared with healthy controls, the fluorescence intensity of T24 was vigorous than LNCaP and PC-3 in tumor cells (Figs. 5A and S8–S12). Additionally, the fluorescence intensity of PC-3 altered mildly after the treatment with Zn^{2+} (Figs. 5A and S5–S9). To further prove our point, TPEN (100 μM) as a Zn^{2+} chelator was added into cells to incubate for 30 min, the fluorescence intensity of TPEN treatment groups were weaken comparing with TPEN untreated groups. This result proved that **H_2L** was specific binding with intracellular Zn^{2+}.

The quantitative fluorescence analysis of each group was conducted to calculate the content of Zn^{2+} accumulation by using ImageJ software. We analyzed the difference of fluorescence intensity between the $ZnCl_2$ treated group and the untreated group to assess the content of the cells for Zn^{2+} accumulation, of note, the quantitative fluorescence analysis should consider the potential factor such as different cells culture medium. The difference outcomes also implied that the prostate healthy epithelial cells RWPE-1 had the most substantial ability for Zn^{2+} accumulation, while the early stage prostate cancer cells LNCaP and the advanced prostate cancer cells PC-3 almost lost their ability to do so (Fig. 5B and 5C). Furthermore, there was no distinct difference in the Zn^{2+} content between the bladder cancer cells T24 and the bladder healthy epithelial cells SV-HUC-1 comparing with the prostate cell lines (Fig. 5C). These results confirmed the close relationship between Zn^{2+} and prostate cancer as reported in the literature and also provided a piece of strong evidence that Zn^{2+} could be used as a diagnostic biomarker for prostate cancer. More importantly, the results showed that the **H_2L** could detect intracellular Zn^{2+} and accurately reflect the Zn^{2+} content in different cells. Then we can easily distinguish healthy cells from cancerous cells according to the comparison of Zn^{2+} content differences, so as to achieve the purpose of diagnosing prostate cancer.

Conclusions

Prostate cancer has a high morbidity rate among male tumor and is challenging to diagnose in the early stage. It was crucial for acquiring the better survival time of patients to diagnose prostate cancer earlier [35]. Many studies reported Zn^{2+} involved in multiple steps of tumorigenesis and deemed to be a biomarker for the prostate cancer diagnosis. In contrast to serum PSA, Zn^{2+}

had more advantage of sensitivity and specificity for prostate cancer rather than any benign prostate disease [2,16]. In order to explore the change of Zn^{2+} level in prostate cancer and healthy tissues, we designed **H_2L**. It is a novel peptide-based reversible fluorescent probe used for the Zn^{2+} detection. This study demonstrated that **H_2L** displayed better sensitivity compared to other Zn^{2+} sensors summarized in Table S3. Also the low toxicity and the superior cell permeability of **H_2L** made the imaging of Zn^{2+} detection safe and rapid. Encouragingly, the **H_2L** can detect intracellular Zn^{2+} and accurately reflect the intracellular Zn^{2+}content. Therefore, we expect that **H_2L** can be a powerful tool for early diagnosis of prostate cancer and an indicator for the precise resection of cancer tissue during surgery.

Declaration of Competing Interest

The authors declare that they have no known competing financial interests or personal relationships that could have appeared to influence the work reported in this paper.

Acknowledgements

This work was supported by the Cuiying Project of Lanzhou University Second Hospital (No. CY2017-BJ05 and CYXZ-23).

Compliance with Ethics Requirements

This article does not contain any studies with human or animal subjects.

Appendix A. Supplementary material

Supplementary data to this article can be found online at https://doi.org/10.1016/j.jare.2020.04.008.

References

[1] McGuire, S, World Cancer Report 2014. Geneva, Switzerland: World Health Organization, International Agency for Research on Cancer, WHO Press, 2015, Adv. Nutr. 7 (2016) 418–9.
[2] Ghosh SK, Pilhan K, Xiao-An Z, Seok-Hyun Y, Anna M, Lippard SJ, et al. A novel imaging approach for early detection of prostate cancer based on endogenous zinc sensing. Cancer Res 2010;70:6119–27.
[3] Chuang AY, Demarzo AM, Veltri RW, Sharma RB, Bieberich CJ, Epstein JI. Immunohistochemical differentiation of high-grade prostate carcinoma from urothelial carcinoma. Am J Surg Pathol 2007;31:1246–55.
[4] Yaghi MD, Kehinde EO. Oral antibiotics in trans-rectal prostate biopsy and its efficacy to reduce infectious complications: Systematic review. Urol Ann 2015;7:417–27.
[5] HB. Carter, American Urological Association (AUA) guideline on prostate cancer detection: process and rationale, BJU. Int, 112 (2013) 543–7.
[6] Lo ST, Martins AF, Jordan VC, Sherry AD. Zinc as an imaging biomarker of prostate cancer. Isr J Chem 2017;57.
[7] Serefoglu EC, Altinova S, Ugras NS, Akincioglu E, Asil E, Balbay MD. 67 How reliable is 12-core prostate biopsy procedure in the detection of prostate cancer?. Eur Urol Suppl 2010;9:54–5.
[8] Catalona WJ, Partin AW, Slawin KM, Brawer MK, Flanigan RC, Patel A, et al. Use of the percentage of free prostate-specific antigen to enhance differentiation of prostate cancer from benign prostatic disease: a prospective multicenter clinical trial. JAMA 1998;279:1542–7.
[9] Cherasse Y, Urade Y. Dietary zinc acts as a sleep modulator. Int J Mol Sci 18 2017:2334-.
[10] Rink L, Gabriel P. Zinc and the immune system. P Nutr Soc 2000;59:541–52.
[11] Franz MC, Anderle P, Burzle M, Suzuki Y, Freeman MR, Hediger MA, et al. Zinc transporters in prostate cancer. Mol Aspects Med 2013;34:735–41.
[12] Clavijo Jordan MV, Lo ST, Chen S, Preihs C, Chirayil S, Zhang S, et al. Zinc-sensitive MRI contrast agent detects differential release of Zn(II) ions from the healthy vs. malignant mouse prostate. Proc Natl Acad Sci USA 2016;113:E5464.
[13] Costello LC, Feng P, Milon B, Tan M, Franklin RB. Role of zinc in the pathogenesis and treatment of prostate cancer: critical issues to resolve, Prostate. Cancer. P. D.; 2004.
[14] Franklin RB, Feng P, Milon B, Desouki MM, Singh KK, Kajdacsyballa A, et al. hZIP1 zinc uptake transporter down regulation and zinc depletion in prostate cancer. Mol Cancer 2005;4:1–13.
[15] Wen C, Zhang DY, Lippard SJ, Radford RJ. Reaction-based fluorescent sensor for investigating mobile Zn2+ in mitochondria of healthy versus cancerous prostate cells. Proc Natl Acad Sci USA 2014;111:143–8.
[16] Costello LC, Franklin RB. Prostatic fluid electrolyte composition for the screening of prostate cancer: a potential solution to a major problem, Prostate. Cancer. P. D. 12 (2009) 17–24.
[17] Sivaraman G, Anand T, Chellappa D. Turn-on fluorescent chemosensor for Zn (II) via ring opening of rhodamine spirolactam and their live cell imaging. Analyst 2012;137:5881–4.
[18] Sivaraman G, Iniya M, Anand T, et al. Chemically diverse small molecule fluorescent chemosensors for copper ion. Coordin Chem Rev 2018;357:50–104.
[19] Sivaraman G, Anand T, Chellappa D. Pyrene based selective–ratiometric fluorescent sensing of zinc and pyrophosphate ions. Anal Methods 2014;6:2343–8.
[20] Vidya B, Sivaraman G, Sumesh RV, et al. Fluorescein-based "turn on" fluorescence detection of Zn2+ and its applications in imaging of Zn2+ in apoptotic cells. ChemistrySelect 2016;1:4024–9.
[21] Ganesan JS, Gandhi S, Radhakrishnan K, et al. Execution of julolidine based derivative as bifunctional chemosensor for Zn(2+) and Cu(2+) ions: Applications in bio-imaging and molecular logic gate. Spectrochim Acta A 2019;219:33–43.
[22] Mariyappan M, Malini N, Sivamani J, et al. Turn-on fluorescence chemosensor for Zn(2+) ion using salicylate based azo derivatives and their application in cell-bioimaging. J Fluoresc 2019;29:737–49.
[23] Karmegam MV, Karuppannan S, Christopher DB, Leslee, et al. Phenothiazine-rhodamine-based colorimetric and fluorogenic 'turn-on' sensor for Zn(2+) and bioimaging studies in live cells. Luminescence 2020;35:90–7.
[24] Wang P, Wu J, Di C, Zhou R, Zhang H, Su P, et al. A novel peptide-based fluorescence chemosensor for selective imaging of hydrogen sulfide both in living cells and zebrafish. Biosens Bioelectron 2016;92:602–9.
[25] Pazos E, Vã zO, Mascareã±As JL, VÃ zquez ME. Peptide-based fluorescent biosensors. Chem Soc Rev 38 (2009) 3348–59.
[26] Wu J, Zou Y, Li C, Sicking W, Piantanida I, Yi T, et al. A molecular peptide beacon for the ratiometric sensing of nucleic acids. J Am Chem Soc 2012;134:1958–61.
[27] Hirayama T, Taki M, Akaoka K, Yamamoto Y. Development of a dual functional luminescent sensor for zinc ion based on a peptidic architecture. Bioorg Med Chem Lett 2012;22:7410–3.
[28] Thirupathi P, Lee KH. A ratiometric fluorescent detection of Zn(II) in aqueous solutions using pyrene-appended histidine. Bioorg Med Chem Lett 2013;23:6811–5.
[29] Wang P, Liu L, Zhou P, Wu W, Wu J, Liu W, et al. A peptide-based fluorescent chemosensor for multianalyte detection. Biosens Bioelectron 2015;72:80–6.
[30] Fu S, Wan X, Du C, et al. A novel fluorescent probe for the early detection of prostate cancer based on endogenous zinc sensing. Prostate 2019;79:1378–85.
[31] Dudev T, Lin YL, Dudev M, Lim C. First-second shell interactions in metal binding sites in proteins: a PDB survey and DFT/CDM calculations. J Am Chem Soc 2003;125:3168–80.
[32] Becke Axel D. Density-functional thermochemistry. I. The effect of the exchange-only gradient correction. J Chem Phys 1992;96:2155–60.
[33] Lee C, Yang W, Parr RG. Development of the Colle-Salvetti correlation-energy formula into a functional of the electron density. Phys Rev B Condens Matter 1988;37:785–9.
[34] Humphrey W, Dalke A, Schulten K. VMD: visual molecular dynamics. J Mol Graph 1996;14:33–8.
[35] Lin DW, Porter M, Montgomery B. Treatment and survival outcomes in young men diagnosed with prostate cancer: a Population-based Cohort Study. Cancer 2010;115:2863–71.